The Differential Roles of Budding Yeast Tem1p, Cdc15p, and Bub2p Protein Dynamics in Mitotic Exit D V

Jeffrey N. Molk,* Scott C. Schuyler,†‡ Jenny Y. Liu,† James G. Evans,§
E. D. Salmon,* David Pellman,† and Kerry Bloom*¶

*Department of Biology, University of North Carolina, Chapel Hill, North Carolina 27599; †Dana-Farber Cancer Institute, Harvard Medical School, Boston, Massachusetts 02115; and §Whitehead Institute, Massachusetts Institute of Technology, Cambridge Massachusetts 02142

In the budding yeast *Saccharomyces cerevisiae* the mitotic spindle must be positioned along the mother-bud axis to activate the mitotic exit network (MEN) in anaphase. To examine MEN proteins during mitotic exit, we imaged the MEN activators Tem1p and Cdc15p and the MEN regulator Bub2p in vivo. Quantitative live cell fluorescence microscopy demonstrated the spindle pole body that segregated into the daughter cell (dSPB) signaled mitotic exit upon penetration into the bud. Activation of mitotic exit was associated with an increased abundance of Tem1p-GFP and the localization of Cdc15p-GFP on the dSPB. In contrast, Bub2p-GFP fluorescence intensity decreased in mid-to-late anaphase on the dSPB. Therefore, MEN protein localization fluctuates to switch from Bub2p inhibition of mitotic exit to Cdc15p activation of mitotic exit. The mechanism that elevates Tem1p-GFP abundance in anaphase is specific to dSPB penetration into the bud and Dhc1p and Lte1p promote Tem1p-GFP localization. Finally, fluorescence recovery after photobleaching (FRAP) measurements revealed Tem1p-GFP is dynamic at the dSPB in late anaphase. These data suggest spindle pole penetration into the bud activates mitotic exit, resulting in Tem1p and Cdc15p persistence at the dSPB to initiate the MEN signal cascade.

INTRODUCTION

In the budding yeast *Saccharomyces cerevisiae* initiation of mitotic exit follows nuclear segregation into the bud. Before anaphase onset cytoplasmic microtubules align the nucleus, containing the mitotic spindle, along the mother-bud axis with one microtubule organizing center, called the spindle pole body (SPB), proximal to the bud neck (Robinow and Marak, 1966; Byers and Goetsch, 1975; Kilmartin and Adams, 1984). The SPB from the previous division segregates to the daughter bud (dSPB) in >95% of cells (Pereira *et al.,* 2001). Microtubule motor proteins, such as Dhc1p, Kip2p, and Kip3p, individually contribute to the specific orientation of the spindle along the mother-bud axis (Li *et al.,* 1993; Yeh

et al., 1995; Miller *et al.,* 1998; Yeh *et al.,* 2000). Time-lapse microscopy has demonstrated anaphase spindle elongation in the mother cell results in a mitotic exit delay until the nucleus repositions along the mother-bud axis (Yeh *et al.,* 1995; Bardin *et al.,* 2000; Bloecher *et al.,* 2000; Daum *et al.,* 2000; Pereira *et al.,* 2000). Thus, a spindle position checkpoint exists to monitor the orientation of the mitotic spindle, ensuring faithful nuclear segregation (Hoyt, 2000).

The spindle position checkpoint includes the Bub2p and Bfa1p two component guanine-activating protein (GAP) complex that inhibits mitotic progression (Alexandru *et al.,* 1999; Fesquet *et al.,* 1999; Li, 1999; Bloecher *et al.,* 2000). Bub2p and Bfa1p localize to both SPBs but preferentially accumulate on the dSPB when spindles are repositioning along the mother-bud axis (Fraschini *et al.,* 1999; Pereira *et al.,* 2000; Pereira *et al.,* 2001). A major target of Bub2p/Bfa1p is the mitotic exit network (MEN), a signal transduction cascade that includes a guanine nucleotide binding protein, Tem1p, and protein kinases such as Cdc15p. Tem1p, Cdc15p, and other MEN proteins asymmetrically localize to the spindle poles (Bardin and Amon, 2001; McCollum and Gould, 2001). The Bub2p/Bfa1p GAP complex is proposed to inhibit the MEN in preanaphase through specific interactions with Tem1p at the dSPB (Geymonat *et al.,* 2002; Ro *et al.,* 2002). After spindle elongation into the bud, Tem1p may be activated by the putative guanine exchange factor (GEF) Lte1p at the bud cell cortex to promote Cdc15p localization to the dSPB, beginning the MEN signal cascade (Bardin *et al.,* 2000; Pereira *et al.,* 2000). In the absence of Bub2p, Tem1p does not localize to the dSPB until late anaphase and Cdc15p localizes before anaphase resulting in inappropriate mitotic

Table 1. *S. cerevisiae* strains

Strain name	Relevant genotype	Source or reference
L 4852	MAT**a** *ade2-100 leu2-3,-112 his3-11,-15 trp1-1 ura3-1*	G. Fink[a]
PY 1973	MAT**a** *ade2-100 leu2-3,-112 his3-11,-15 trp1-1 ura3-1 ase1Δ::KAN*	Lee et al. (1999)
PY 2370	MAT**a** *ade2-100 ade3 leu2-3,-112 his3-1,-15 trp1-1 ura3-1 TUB1::GFP-URA3*	Tirnauer et al., (1999)
PY 3446	MAT**a** *ade2-100 leu2-3,-112 his3-11,-15 trp1-1 ura3-1 ase1Δ::KAN TUB1::GFP-URA3*	Schuyler et al., (2003)
PY 3548	MAT**a** *ade2-100 leu2-3,-112 his3-11,-15 trp1-1 ura3-1 LTE1::3×GFP-URA3*	This study
YEF 473A	MAT**a** *trp1Δ63 leu2Δ1 ura3-52 his3Δ200 lys2-801*	Bi and Pringle (1996)
KBY 9201	MAT**a** *trp1Δ63 leu2Δ1 ura3-52 his3Δ200 lys2-801 TEM1::GFP-KAN*	This study
KBY 9202	MAT**a** *trp1Δ63 leu2Δ1 ura3-52 his3Δ200 lys2-801 CDC15::GFP-KAN*	This study
KBY 9203	MAT**a** *trp1Δ63 leu2Δ1 ura3-52 his3Δ200 lys2-801 TEM1::GFP-HB*	This study
KBY 9205	MAT**a** *trp1Δ63 leu2Δ1 ura3-52 his3Δ200 lys2-801 kar9Δ::HB TEM1::GFP-KAN*	This study
KBY 9208	MAT**a** *trp1Δ63 leu2Δ1 ura3-52 his3Δ200 lys2-801 dhc1Δ::HIS3 TEM1::GFP-KAN*	This study[b]
KBY 9209	MAT**a** *trp1Δ63 leu2Δ1 ura3-52 his3Δ200 lys2-801 SPC29::GFP-KAN*	This study
KBY 9211	MAT**a** *trp1Δ63 leu2Δ1 ura3-52 his3Δ200 lys2-801 kip2Δ::KAN TEM1::GFP-HB*	This study
KBY 9212	MAT**a** *trp1Δ63 leu2Δ1 ura3-52 his3Δ200 lys2-801 kip3Δ::KAN TEM1::GFP-HB*	This study
KBY 9217	MAT**a** *trp1Δ63 leu2Δ1 ura3-52 his3Δ200 lys2-801 lte1Δ::HB TEM1::GFP-KAN*	This study
KBY 9221	MAT**a** *trp1Δ63 leu2Δ1 ura3-52 his3Δ200 lys2-801 BUB2::GFP-KAN*	This study
KBY 9225	MAT**a** *trp1Δ63 leu2Δ1 ura3-52 his3Δ200 lys2-801 bud6Δ::TRP1 TEM1::GFP-KAN*	This study[c]
KBY 9228	MAT**a** *trp1Δ63 leu2Δ1 ura3-52 his3Δ200 lys2-801 CDC15::GFP-KAN TUB1::CFP-URA3*	This study
KBY 9233	MAT**a** *trp1Δ63 leu2Δ1 ura3-52 his3Δ200 lys2-801 dhc1Δ::HIS3 BUB2::GFP-KAN*	This study[b]
KBY 9234	MAT**a** *trp1Δ63 leu2Δ1 ura3-52 his3Δ200 lys2-801 lte1Δ::HB BUB2::GFP-KAN*	This study
KBY 9248	MAT**a** *trp1Δ63 leu2Δ1 ura3-52 his3Δ200 lys2-801 ase1Δ::HB TEM1::GFP-KAN*	This study

[a] Whitehead Institute, Cambridge, MA.
[b] Parent strain provided by D. Beach, University of North Carolina, Chapel Hill, NC.
[c] Parent strain provided by J. Pringle, University of North Carolina, Chapel Hill, NC.

exit if spindle abnormalities exist (Hoyt *et al.,* 1991; Pereira *et al.,* 2000; Visintin and Amon, 2001). These data suggest Bub2p influences the localization of upstream MEN components at the dSPB.

The asymmetric localization of MEN components has led to a spatial separation mechanism for MEN function (Bardin *et al.,* 2000; Pereira *et al.,* 2000). If the spindle is not positioned along the mother-bud axis the dSPB will not enter the bud and mitotic exit will be delayed by Bub2p-Bfa1p GAP inactivation of Tem1p. Entry of the dSPB into the bud places Tem1p in the same compartment as Lte1p to activate mitotic exit. However, Lte1p GEF activity is required for Lte1p localization at the bud cortex but is not essential for mitotic exit (Yoshida *et al.,* 2003). Furthermore, Lte1p is not required for mitotic exit at physiological temperatures (Shirayama *et al.,* 1994; Adames *et al.,* 2001). A second mechanism for mitotic exit may involve negative regulation by cytoplasmic microtubules (Adames *et al.,* 2001). In this model, mitotic exit proceeds only when cytoplasmic microtubule connections with the bud neck are lost. The spatial separation and cytoplasmic microtubule models are not mutually exclusive and it is possible that both dSPB penetration into the bud and loss of cytoplasmic microtubules at the bud neck are required for cells to exit mitosis.

Models for mitotic exit have not incorporated either the spatial or the temporal regulation of MEN protein localization in living cells. Is there an event associated with spindle elongation, such as dSPB penetration into the bud or dSPB contact with the distal bud cortex, that correlates with mitotic exit? If so, how do the early MEN components Tem1p and Cdc15p localize in response to the initiating event for mitotic exit? Does the MEN inhibitor Bub2p alter its localization on the dSPB during mitotic exit? Do MEN proteins such as Tem1p exchange with the cytoplasmic protein pool? Finally, can Lte1p or regulators of spindle positioning affect the localization of Tem1p on the dSPB?

To investigate these questions, we have used quantitative live cell imaging of fluorescence fusion proteins and measurements of fluorescence recovery after photobleaching (FRAP). The initiating signal for mitotic exit is dSPB penetration into the bud. Additionally, Tem1p-GFP and Cdc15p-GFP persistently accumulate on the dSPB upon bud neck penetration, whereas Bub2p-GFP fluorescence intensity declines in mid-to-late anaphase. Tem1p-GFP on the dSPB is dynamic in late anaphase, indicating the accumulation of Tem1p during anaphase does not result in tight binding to the dSPB. The major increase in Tem1p-GFP fluorescence on the dSPB occurs specifically in the bud compartment and Tem1p-GFP abundance is promoted by the minus-end microtubule motor protein dynein (Dhc1p) and Lte1p. Thus, activation of mitotic exit causes a change in MEN protein abundance and persistence upon dSPB penetration of the bud that drives the progression to interphase.

MATERIALS AND METHODS

Media and Strain Construction

Media and genetic techniques are described elsewhere (Rose and Broach, 1990). Geneticin (Life Technologies, Invitrogen Co., Carlsbad, CA) or hygromycin B (CellGro Co., Herndon, VA) was used at a concentration of 0.2 or 0.4 μM in YPD. α-factor (Research Genetics, Invitrogen Co., Carlsbad, CA) was used at a final concentration of 10 μg/ml. PCR primer sequences are listed in Supplementary Table 1 and *S. cerevisiae* strains used in this study are listed in Table 1.

A wild-type strain expressing GFP-Tub1p (PY 2370) was mated with an *ase1Δ* strain (PY 1973) to generate PY 3446 (Sikorski and Hieter, 1989; Lee *et al.,* 1999; Tirnauer *et al.,* 1999). pB1594 integrated three tandem copies of GFP at the 3′ end of the *LTE1* coding region (Lte1p-3xGFP). The growth of this strain was tested at 14°C and 37°C, and it was similar to wild-type (Supplementary Figure 1A). The Lte1p-3xGFP construct complemented the cold sensitivity of *lte1Δ* and *ase1Δ lte1Δ* synthetic lethality at 37°C (Supplementary Figure 1, A and B).

Fusion of GFP to the 3′ ends of *TEM1, BUB2,* and *CDC15* was constructed by PCR fragment–mediated transformation using the pFA6::*GFP-KANMX* template (Wach *et al.,* 1994). The resulting strains exhibited wild-type growth

rates, indicating neither Tem1p nor Cdc15p function were compromised (Supplementary Figure 2A). Similarly, none of the strains were benomyl sensitive, suggesting the spindle position checkpoint was not abrogated (Supplementary Figure 2B). Gene disruptions were made using PCR fragment-mediated transformation conferring antibiotic resistance (Wach *et al.,* 1994; Longtine *et al.,* 1998; Goldstein and McCusker, 1999). All integrations were confirmed by PCR. Cyan fluorescence protein (CFP)-Tub1p plasmid, derived from pAFS125 (Straight *et al.,* 1997), was linearized with *Stu*I before transformation.

Timing of Mitotic Exit Image Acquisition and Data Analysis

Liquid log phase *ASE1* and *ase1Δ* strains expressing GFP-Tub1p were treated with α-factor for 2 h at 30°C (90% shmoos), released into fresh medium, washed, and imaged 40–50 min later as detailed in Tirnauer *et al.* (1999). Time-lapse movies were made at 25°C by acquiring alternating differential interference contrast (DIC) and epi-fluorescence images in 17 Z-planes of 0.3-μm steps (2 × 2 binning) every 2 min. Six hundred-millisecond fluorescence exposure times were used with seven-eighths of the excitation light attenuated by a neutral density filter. DIC exposures were for 30 ms. Fluorescence Z-series from each time point were merged and analyzed as a single projection superimposed on the corresponding DIC image. All image manipulations and measurements were made using Openlab Software v3.0.2 (Improvision, Lexington, MA).

The first image after clear spindle penetration into the bud was designated as $t = 0$ min for measuring mitotic exit events. This criterion results in a number of instances where the spindle pole is within the bud volume at $t = 0$ min. Thus, the resolution of our imaging is 2 min. A cortical interaction was scored when the spindle pole body was ≤0.5 μm from the side of the bud cortex in either a stationary position or a brushing-sweeping motion in two consecutive images. Cells where cortical contact may have occurred at the top or bottom of the cell were omitted. Spindle elongation rates were determined by linear regression of two to four time points from a 1.5–2-μm to a 4–6-μm bipolar spindle for the fast phase of spindle elongation and two to eight time points from a 4–6-μm to a 8–12-μm spindle for the slow phase of spindle elongation. Septation was scored as the rotation of the daughter and mother cells relative to one another in DIC images (Yeh *et al.,* 1995; Bi *et al.,* 1998). Measurements were exported to Microsoft Excel (Microsoft Co., Seattle, WA) and statistical comparisons were made using Statview (SAS Institute Inc., Cary, NC) and Kaleidagraph 3.0.4 (Abelbeck Software, Reading, PA).

Native Level Lte1p-3xGFP Localization

Midlogarithmically growing Lte1p-3xGFP–expressing cells mixed with wild-type untransformed cells were imaged by acquiring 80 plane Z-stacks at 0.2-μm steps (1 × 1 binning) with 2-s epi-fluorescence exposures and 30-ms transillumination exposures. Images were deconvolved using 500 iterations an Accelerated-Maximum-Likelihood-Estimation restoration algorithm optimized for low light imaging in Huygens2 (Scientific Volume Imaging, Hilversum, Netherlands). Autofluorescence was subtracted using the nearby untransformed wild-type cells. The data were rendered using the "Simulated Fluorescence Process" algorithm within Imaris3 (Bitplane, Zurich, Switzerland).

Live Cell Analysis of MEN Fluorescence Fusion Proteins

Midlogarithmic phase cells expressing Tem1p-GFP, Bub2p-GFP, Cdc15p-GFP, and CFP-Tub1p were imaged as described elsewhere (Shaw *et al.,* 1997a; Maddox *et al.,* 2000). Image processing was performed with Meta-Morph software (Universal Imaging Co., West Chester, PA). Three- or five-plane Z-series at 0.75-μm steps (2 × 2 binning) were acquired every 2 min with 400-ms epi-fluorescence exposures and a single 100-ms DIC exposure (1 × 1 binning). For two color imaging, the yellow fluorescence protein (YFP) epi-fluorescence exposure time was 500 ms, and the CFP epi-fluorescence exposure time was 350 ms.

MEN Fluorescence Fusion Protein Image Analysis

Three-dimensional stacks of Tem1p-GFP, Bub2p-GFP, Cdc15p-GFP, or CFP-Tub1p time-lapse movies were compiled into a single maximum projection for each time point (Shaw *et al.,* 1997a). Fluorescence intensity measurements were made by placing a 35–40 pixel² circle around a Tem1p-GFP or Bub2p-GFP signal and the integrated intensity was recorded to a linked Microsoft Excel spreadsheet. The mSPB fluorescence intensities of Tem1p-GFP are over-estimates because cells with no mSPB fluorescence were not measured. Background fluorescence was subtracted by placing the same measurement circle in three different nearby intracellular regions without a Tem1p-GFP or Bub2p-GFP signal and the three measurements were averaged to give a single data point for each time interval. Three-dimensional static images, where a single five-plane Z-series at 0.75-μm steps was acquired, were not compiled; the brightest signal from the five planes was used to generate the single data point. To determine the stage of mitosis, bud size and position of the SPB relative to the bud neck were used. A signal proximal to the bud neck was scored as preanaphase; a signal moving toward the daughter cortex or in

between the bud neck and daughter cell cortex was scored as anaphase spindle elongation; a signal directly adjacent to the daughter cell cortex was scored as late anaphase. Student's two-tailed *t* test was used for all statistical analysis, and $p < 0.01$ was considered significant.

For Tem1p-GFP fluorescence intensity measurements during anaphase, nine living cells were imaged as above (no binning) and three-plane Z-series were compiled. Each dSPB was measured for fluorescence intensity and distance from the Tem1p-GFP signal to the center of the bud neck using Track Points in MetaMorph. All measurements were averaged and at least two measurements were used for each time point. Spindle length was recorded using the linear calibrated distance between two Tem1p-GFP foci. Anaphase onset was marked at $t = 0$ min and any time before anaphase onset was denoted as a negative value (i.e., $t = -8$ min). Single Bub2p-GFP cells were analyzed similarly using 2 × 2 binned images of compiled five-plane Z-series.

FRAP of Tem1p-GFP

FRAP experiments were performed as detailed elsewhere (Maddox *et al.,* 2000; Kosco *et al.,* 2001). Cells were photobleached with a 35-ms laser pulse. For Tem1p-GFP a single focal plane with a 400-ms epi-fluorescence exposure time was obtained for three data points before photobleaching and 10 data points after photobleaching at 3-s intervals followed by 10 data points obtained at 10-s intervals, and then four to six data points at 30-s intervals. Thus, each recovery was measured for ~270 s. Aperiodic DIC images (100-ms exposure time) were acquired for each experiment as well. Recovery was not significantly altered by photobleaching due to image acquisition for up to 30 frames acquired in unbleached cells (our unpublished results). A 5 × 5-pixel box was used to make fluorescence intensity measurements. Intracellular background was subtracted according to the methods above and three measurements were averaged for each data point. Dividing the dSPB fluorescence intensity measured immediately after photobleaching by the fluorescence intensity before photobleaching indicated an average of 4% of Tem1p-GFP remained unbleached at the dSPB before recovery (our unpublished results).

Fluorescence recovery, or the loss of bleached fluorescence at the dSPB, was initially analyzed by assuming a single rate constant as follows (Salmon *et al.,* 1984; Saxton *et al.,* 1984; Wadsworth and Salmon, 1986):

$$F_\infty - F(t) = [F_\infty - F(0)]e^{-kt}, \tag{1}$$

where F_∞ is the average intensity of the bleached region after maximum recovery, $F(t)$ is the fluorescence intensity at each time point ($t = 0$ s was immediately after photobleaching), $F(0)$ is the fluorescence intensity at $t = 0$ s, k is the rate constant for exponential decay, and t is time. The natural logarithm of the quantity on the left side of the following equation derived from (Eq. 1):

$$\frac{F_\infty - F(t)}{F_\infty - F(0)} = e^{-kt}, \tag{2}$$

was plotted vs. time for analysis. A single straight line on this logarithmic plot predicts a single rate constant but the two slopes for Tem1p-GFP indicated a fast recovery fraction and a slow recovery fraction. To analyze the biphasic nature of bleached subunit disassociation, the data from Eq. 2 that generated the logarithmic plot were exported to SigmaPlot 8.0 (SPSS Science, Chicago, IL) and analyzed using the Exponential Decay function (Double, 4 Parameter) for two rate constants that follow from the formula:

$$\frac{F_\infty - F(t)}{F_\infty - F(0)} = f_f*(e^{-k_f t}) + f_s*(e^{-k_s t}), \tag{3}$$

where the fast phase and slow phase rate constant (k_f and k_s), and the fraction of recovery due to the fast and slow phases (f_f and f_s) were calculated. Using these rate constants and recovery values we generated a best-fit biphasic recovery curve for the theoretical association of unbleached subunits to the dSPB with the formula:

$$F(t)=F(0)+f_f*(F_\infty-F(0))*(1-e^{-k_f\Delta t})+f_s*(F_\infty-F(0))*(1-e^{-k_s\Delta t}), \tag{4}$$

where $\Delta t = t - t_0$. The best-fit data for single and biphasic recovery were plotted separately from the experimental data for comparison.

To determine the fraction of Tem1p-GFP that recovers to the dSPB within the imaging interval, we calculated the fluorescence recovery ratio, R (Howell *et al.,* 2000):

$$R = \frac{F_\infty - F(0)}{F_{pre*} - F(0)}. \tag{5}$$

The fluorescence intensity before photobleaching (F_{pre*}) was determined by multiplying each of the three fluorescence intensity measurements before photobleaching ($F(t)_{pre}$) by the ratio of total cellular fluorescence intensity immediately after photobleaching (F_{c-post}) to the total cellular fluorescence intensity immediately before photobleaching (F_{c-pre}):
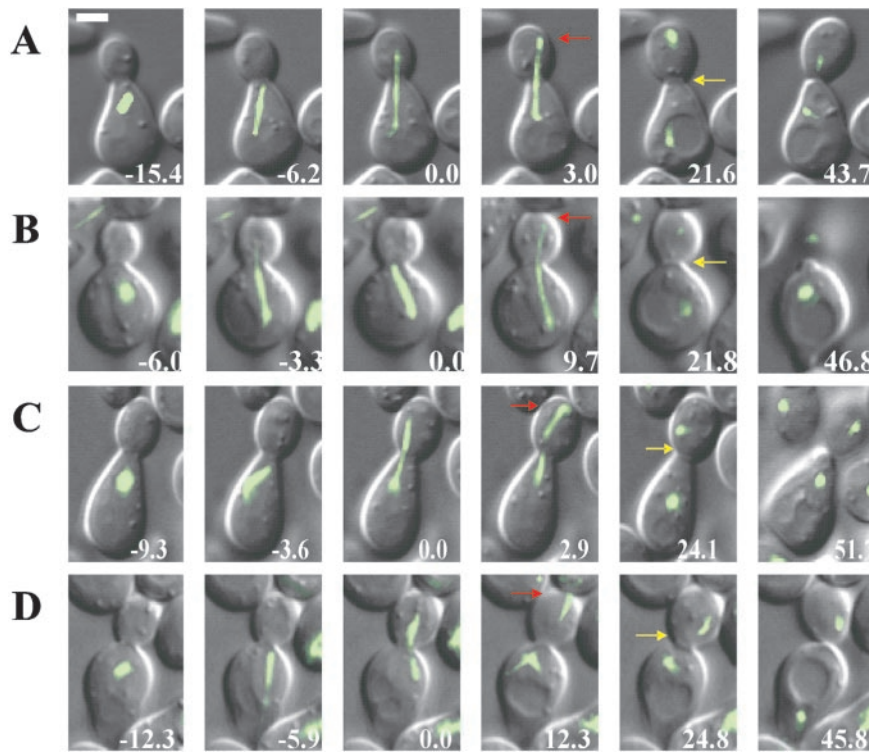
Figure 1. Time-lapse series of anaphase in haploid wild-type (A and B) and *ase1Δ* mutant (C and D) cells expressing a GFP-Tub1p (Bar, 2 μm). (A) An example of an early contact event between the SPB and the distal bud cortex, relative to the mean value of the population, in a wild-type cell. Early spindle pole body-cortical contact (3.0 min, red arrow), septation (21.6 min, yellow arrow), and cell separation (43.7 min) from the time of spindle pole body entry into the bud (0.0 min). (B) An example of a late contact event between the SPB and the distal bud cortex, relative to the mean population value, in a wild-type cell. Late spindle pole body-cortical contact (9.7 min, red arrow), septation (21.8 min, yellow arrow), and cell separation (46.8 min) from the time of spindle pole body entry into the bud (0.0 min). (C) An example of an early contact event in an *ase1Δ* cell. Early spindle pole body-cortical contact (2.9 min, red arrow), septation (24.1 min, yellow arrow), and cell separation (51.7 min) from the time of spindle pole body entry into the bud (0.0 min). (D) An example of a late contact event in an *ase1Δ* cell. Late spindle pole body-cortical contact (12.3 min, red arrow), septation (24.8 min, yellow arrow), and cell separation (45.8 min) from the time of spindle pole body entry into the bud (0.0 min).

$$F(t)_{\text{pre-corr}} = F(t)_{\text{pre}} * \frac{F_{\text{c-post}}}{F_{\text{c-pre}}}. \qquad (6)$$

The three corrected fluorescence intensity values ($F(t)_{\text{precorr}}$) were averaged to a single prebleach data point ($F_{\text{pre*}}$) used in Eq. 5. This will correct for the fraction of Tem1p-GFP fluorophore in the total protein pool destroyed by the laser pulse during photobleaching and averaged 20% in each experiment.

RESULTS

Spindle Pole Body Passage through the Bud Neck Signals Mitotic Exit

A connection between spindle morphology during anaphase and mitotic exit has not been established. We analyzed wild-type cells expressing GFP-Tub1p to determine if there is an event associated with spindle elongation that correlates with mitotic exit (Figure 1, A and B). The average time from dSPB passage through the bud neck to contact with the distal bud cortex was 6 min (Figure 2A), and the mean interval from dSPB-cortical contact to septation was 16 min (Figure 2B). The time from dSPB penetration into the bud to septation was 22 min (Figure 2C), demonstrating a strict temporal link between dSPB entry into the bud, completion of mitotic exit, and septation.

dSPB penetration into the bud is coincident with spindle elongation. Using *ase1Δ* cells that exhibit premature spindle breakdown in early anaphase (Pellman *et al.,* 1995; Schuyler *et al.,* 2003), we tested if there is a requirement for a stable anaphase spindle to signal mitotic exit. The behavior of spindle poles in *ase1Δ* mutants was similar to wild-type cells (Figure 1, C and D). The mean intervals between dSPB entry into the bud and cortical contact, cortical contact and septation, and entry into the bud and septation were indistinguishable in *ase1Δ* cells when compared with wild-type (Figure 2, A–C; wild-type: n = 56; *ase1Δ*: n = 50). Thus, dSPB penetration into the bud signals mitotic exit.

To test whether dSPB penetration into the bud compartment or direct contact between the dSPB and the bud cortex distal from the bud neck signals mitotic exit, we determined if there was a significant correlation between dSPB entry into the bud, distal cortical contact, and septation. If there is a direct correlation between the timing of any two of these events, the slope of the best-fit line should equal 1; if the events are not correlated the slope will be 0. The timing of dSPB entry into the bud to the first contact with the distal bud cell cortex does not correlate with the timing of dSPB entry into the bud to septation (0.086 ± 0.212, Figure 2D). Therefore septation does not correlate with dSPB-distal cortical contact.

Because the interval between dSPB entry into the bud and septation is essentially invariant (Figure 2C), a longer interval from dSPB penetration into the bud to distal cortical contact predicts a shorter interval between distal cortical contact and septation or a negative correlation. The timing of dSPB entry of the bud to distal cortical contact vs. the timing of distal cortical contact to septation was negatively correlated (−0.914 ± 0.212; Figure 2E). Therefore, dSPB entry into the bud triggers septation. Moreover, the total amount of time the dSPB spends in contact with the daughter cell cortex as a percentage of the total time the dSPB spends within the bud does not predict the timing of septation (0.000 ± 0.066; Figure 2F). Similarly, *ase1Δ* cells showed neither a relationship between the time of initial dSPB-distal cortical contact and septation (0.192 ± 0.219; Figure 2G) nor between the percentage of time the dSPB contacted the cell cortex and septation (−0.005 ± 0.093; Figure 2H). Together these data provide strong evidence that dSPB penetration into the bud, and not dSPB-distal cortical contact or stable anaphase spindle elongation, triggers mitotic exit.

Tem1p-GFP Distribution Changes during Spindle Positioning and Spindle Elongation

The accumulation of Tem1p on the dSPB during mitosis could link spindle alignment and dSPB passage into the bud
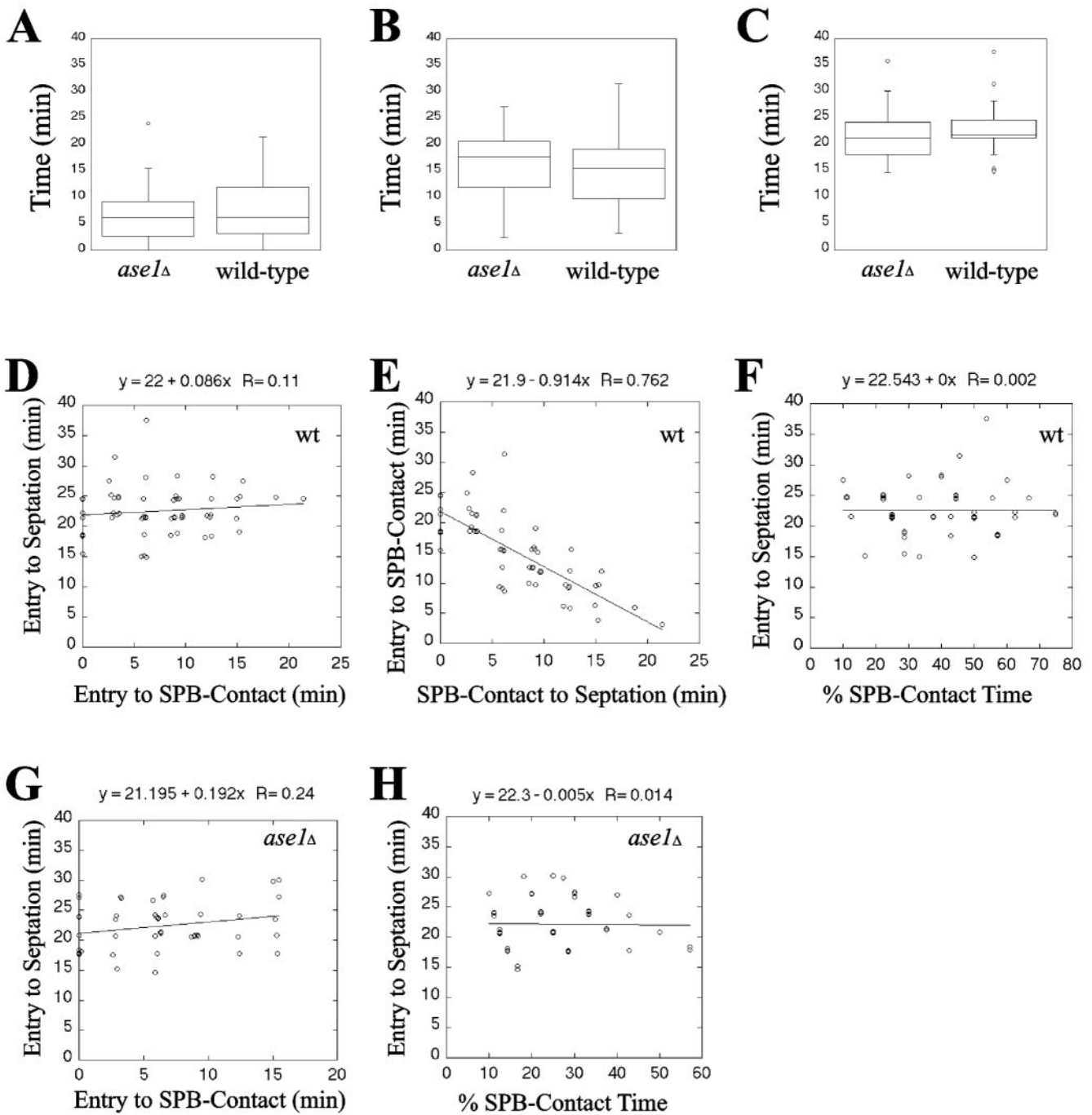
Figure 2. The timing of mitotic exit correlates best with entry of the daughter spindle pole body into the bud and is not affected by premature spindle collapse. The box plots in A to C display the upper and lower quartiles as the boundaries of the box with the horizontal line inside the box denoting the median. The whiskers indicate the boundaries of the outliers which are represented by small circles and were defined by data greater than the quantity (upper quartile + [1.5*interquartile distance]) or less than (lower quartile − [1.5*interquartile distance]). wt denotes wild-type cells analyzed. n = 56 wt cells and 50 *ase1*Δ cells. (A) The time of spindle pole body entry into the bud to cortical contact is not different in an *ase1*Δ mutant compared with wild-type (p = 0.3408 < 0.9500). (B) The time of daughter cell cortical contact to septation is not different in an *ase1*Δ mutant from wild-type (p = 0.4408 < 0.9500). (C) The timing of spindle pole body entry into the bud to septation in an *ase1*Δ mutant is not different from wild-type (p = 0.8773 < 0.9500). (D) There is no correlation between spindle pole body contact with the bud cortex and the timing of the initiation of septation in wild-type cells (slope of 0.086 ± 0.212; mean ± SE). (E) There is negative correlation between the timing of spindle pole body contact with the bud cortex and the time between cortical contact and the initiation of septation in wild-type cells (slope of −0.914 ± 0.212). (F) There is no correlation between the duration of the spindle pole body contact with the bud cortex and the initiation of septation in wild-type cells (slope of 0.000 ± 0.066). (G) There is no correlation between spindle pole body contact with the bud cortex and the initiation of septation in *ase1*Δ cells (slope of 0.192 ± 0.219). (H) There is no correlation between the duration of the spindle pole body contact with the bud cortex and the initiation of septation in *ase1*Δ cells (slope of −0.005 ± 0.093).
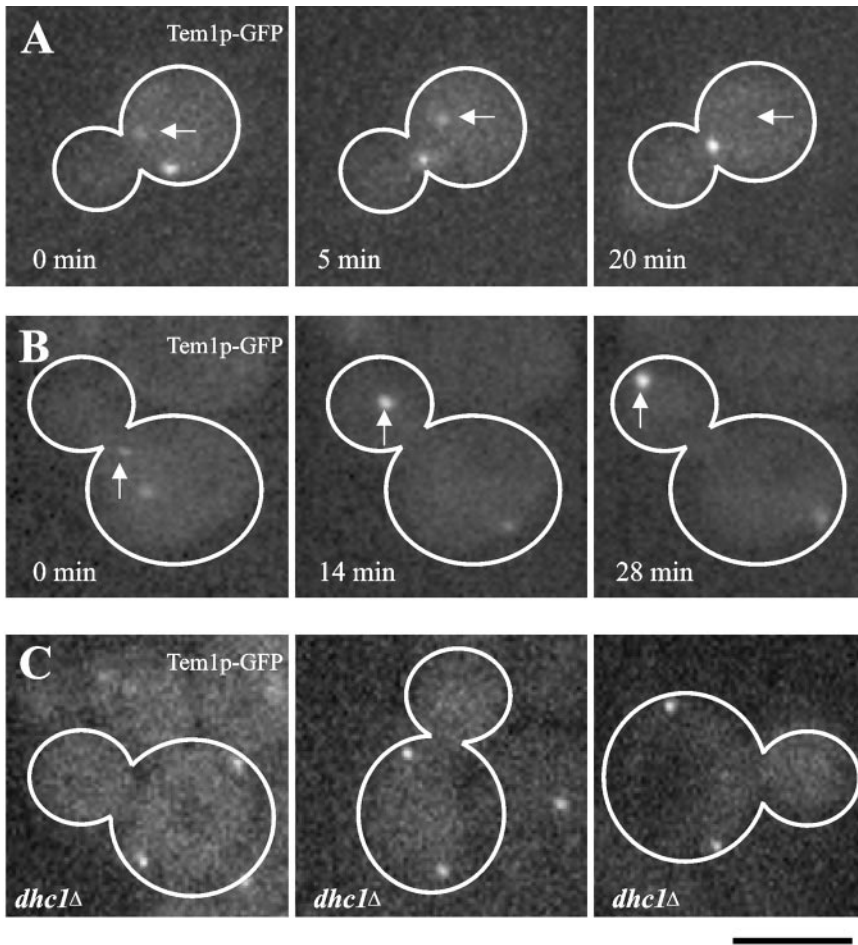
Figure 3. Tem1p-GFP accumulates in response to spatial positioning during mitosis (Bar, 5 μm). (A) Cell undergoing spindle rotation before anaphase expressing Tem1p-GFP. Arrow indicates mSPB. (0 min) The mitotic spindle is oriented parallel to the bud neck and one SPB was preferentially labeled with Tem1p-GFP. (5 min) Spindle positioning altered Tem1p-GFP fluorescence intensity. (20 min) As spindle rotation is completed Tem1p-GFP clearly localized preferentially to the dSPB. (B) Tem1p-GFP localization during anaphase elongation of the mitotic spindle. Arrow denotes dSPB. (0 min) Tem1p-GFP labeled the mSPB at an apparent equal intensity to Tem1p-GFP on the dSPB. (14 min) On spindle elongation Tem1p-GFP was dim on the mSPB but intensely labeled the dSPB. (28 min) Tem1p-GFP appeared to increase in fluorescence intensity in late anaphase on the dSPB. (C) Three representative *dhc1Δ* cells expressing Tem1p-GFP with elongated spindles in the mother cell.

with activation of the MEN. To examine the localization and dynamics of Tem1p, GFP was fused to the 3′ end of the endogenous *TEM1* locus. In cells where the spindle has not aligned along the mother-bud axis Tem1p-GFP often localized preferentially to one SPB that subsequently positioned on the mother side of the bud neck (Figure 3A). This asymmetric accumulation was usually maintained until anaphase onset. However, in a small fraction of cells, both SPBs were labeled equally with Tem1p-GFP in preanaphase (Figure 3B, 0 min). Anaphase onset in all wild-type Tem1p-GFP expressing cells resulted in a fluorescence intensity increase on the dSPB in the bud (Figure 3B, Supplementary Movie 1). After spindle breakdown Tem1p-GFP was lost from the dSPB and was not detected at any other structure in the cell (our unpublished results). Tem1p-GFP on the mSPB localized at least transiently in >80% of living cells during spindle alignment and/or spindle elongation, indicating Tem1p localizes to both SPBs before and during mitotic exit activation.

To quantitate the levels of Tem1p-GFP on spindle poles in wild-type cells, we measured the fluorescence intensity of Tem1p-GFP during mitosis for cells imaged in three dimensions in the population and over time (see Table 2 for summary of all fluorescence intensity measurements). On average Tem1p-GFP was more intense on the dSPB, indicating Tem1p-GFP preferentially accumulated on the SPBs that entered the daughter cell during mitosis (Figure 4A). In addition, Tem1p-GFP increased in fluorescence intensity on dSPBs as spindles elongated (Figure 4A). By late anaphase Tem1p-GFP was two times as intense on the

Table 2. Summary of fluorescence intensity measurements

SPB measured[a]	Genetic background	Fluorescence ratio[b]	p
	Spc29p-GFP		
dSPB (PA vs. LA)[c]	Wild-type	1:1.34	>0.05
mSPB (PA vs. LA)	Wild-type	1:1.03	>0.10
	Tem1p-GFP		
dSPB (PA vs. LA)	Wild-type	1:2.02	**<10⁻⁶ᵈ**
mSPB (PA vs. LA)	Wild-type	1:1.41	<0.05
dSPB	Δ*ase1*	1.08:1	>0.10
dSPB	Δ*lte1*	0.54:1	**<10⁻⁷**
dSPB	Δ*kar9*	0.76:1	<0.02
dSPB	Δ*bud6*	1.00:1	>0.10
dSPB	Δ*dhc1*	0.63:1	**<10⁻⁴**
dSPB	Δ*kip2*	0.72:1	<0.02
dSPB	Δ*kip3*	1.43:1	**<0.01**
	Bub2p-GFP		
dSPB (PA vs. LA)	Wild-type	1.03:1	>0.10
dSPB (PA)	Δ*lte1*	1.10:1	>0.10
dSPB (LA)	Δ*lte1*	0.88:1	>0.10

[a] Late anaphase spindle pole measured unless noted.
[b] Mutant vs. wild-type ratio reported unless indicated otherwise.
[c] PA, preanaphase spindle pole measured; LA, late anaphase spindle pole measured.
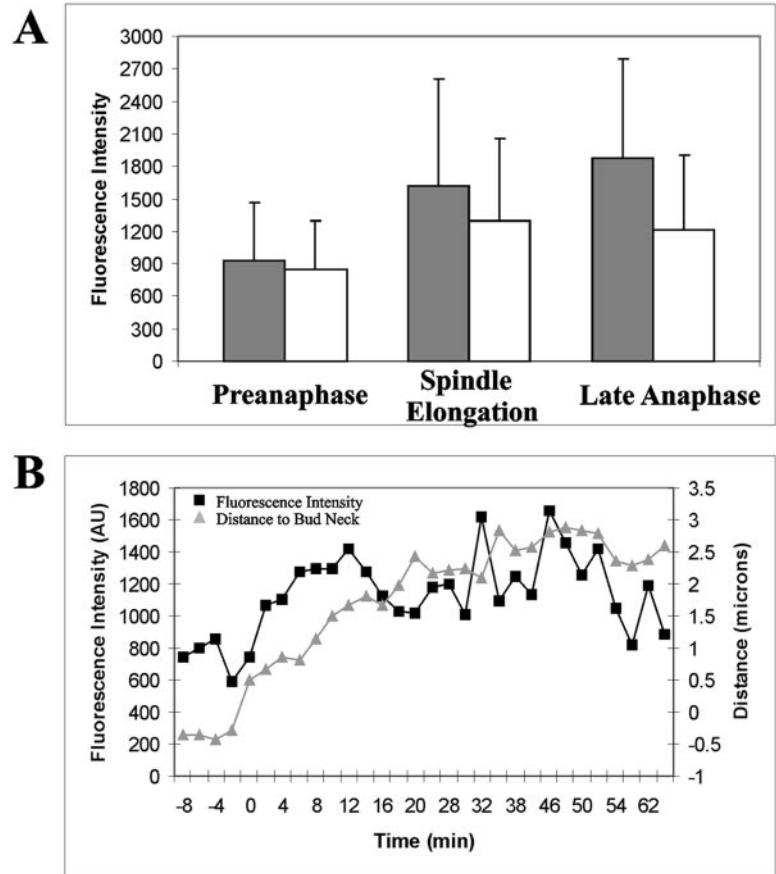[d] Bold type denotes statistically significant difference.

Figure 4. Fluorescence intensity measurements of Tem1p-GFP. (A) Fluorescence intensity measurements of Tem1p during mitosis. mSPBs are overestimated as those cells with no mSPB focus were not accounted for. Error bars indicate SD for each measurement. dSPB (■): n = 38 (preanaphase), 23 (spindle elongation), and 50 (late anaphase). mSPB (□): n = = 20 (preanaphase), 27 (spindle elongation), and 39 (late anaphase). (B) Average distance and intensity measurements for Tem1p-GFP of nine cells during spindle elongation. Black squares, average relative Tem1p-GFP fluorescence intensity in arbitrary units (AU); gray triangles, average distance from the Tem1p-GFP focus to the center of the bud neck in microns. Spindle lengths based on distance from dSPB to transient mSPBs labeled with Tem1p-GFP: preanaphase, 1.99 μm; 0–10 min, 3.47 μm; 12–20 min, 5.14 μm; 22–30 min, 5.83 μm; and $\geq$32 min, 6.84 μm.

dSPB, a significant difference from preanaphase cells (p < 1 × 10^{-6}). Tem1p-GFP did not significantly increase on the mSPB from preanaphase to late anaphase (p > 0.10). As a control, we measured the structural SPB component Spc29p and found Spc29p-GFP does not double in fluorescence intensity on either SPB during mitosis (p > 0.05). Recording individual cells progressing through mitosis demonstrated that the increase in Tem1p-GFP fluorescence intensity closely followed dSPB penetration into the daughter cell (Figure 4B). The fluorescence signal peaked in late anaphase when the spindle reached maximum elongation. The mSPB Tem1p-GFP signal was variable during spindle elongation and did not display a consistent localization pattern preventing analysis similar to the dSPB.

The increase in Tem1p-GFP on the dSPB during spindle elongation could be due to spindle pole penetration into the bud or could be a consequence of anaphase onset. To distinguish between these possibilities, we deleted the dynein heavy chain (DHC1), resulting in a fraction of cells where the spindle does not align along the mother-bud axis and anaphase spindle elongation occurs entirely within the mother cell (Li *et al.*, 1993; Yeh *et al.*, 1995). In *dhc1*Δ mutants where the spindle was elongated within the mother cell, Tem1p-GFP labeled both SPBs and did not display the increased asymmetric fluorescence intensity characteristic of wild-type spindle elongation (Figure 3C). Together, these data suggest as anaphase proceeds Tem1p accumulates and persists at the dSPB upon penetration into the daughter cell.

Cdc15p Localization Coincides with Spindle Elongation in Anaphase

If the MEN is activated when Tem1p-GFP fluorescence increases, then the downstream protein kinase Cdc15p should accumulate at the dSPB upon penetration into the bud. We constructed a strain expressing Cdc15p-GFP as well as CFP-Tub1p to determine the accumulation of Cdc15p at the dSPB relative to spindle elongation into the bud. Cdc15p-GFP accumulated at the dSPB 4 min after anaphase onset when the dSPB began to penetrate the bud neck (Figure 5B, 4 min). The mSPB was not labeled with Cdc15p-GFP during early anaphase, indicating that the initial localization of Cdc15p-GFP is specific for penetration of the bud. As anaphase proceeded, Cdc15p-GFP continued to accumulate on the dSPB and also localized to the mSPB (Figure 5B, 16 and 24 min). Therefore, the timing of Cdc15p localization to the dSPB coincided both with the increase in Tem1p accumulation after anaphase onset and dSPB penetration into the bud.

Bub2p-GFP Decreases on the dSPB during Late Anaphase

When the MEN is activated, does the localization of Bub2p change in living cells? In wild-type cells both Tem1p-GFP and Cdc15p-GFP increase in fluorescence intensity on the dSPB during anaphase (Figures 3 and 5). To determine if Bub2p localization is altered during anaphase, GFP was fused to the C-terminus of Bub2p. Bub2p-GFP increased in fluorescence intensity on the dSPB during anaphase spindle elongation and then decreased in fluorescence intensity in late anaphase (Figure 6A; Supplementary Movie 2). Bub2p-GFP fluorescence intensity on the mSPB was lost soon after
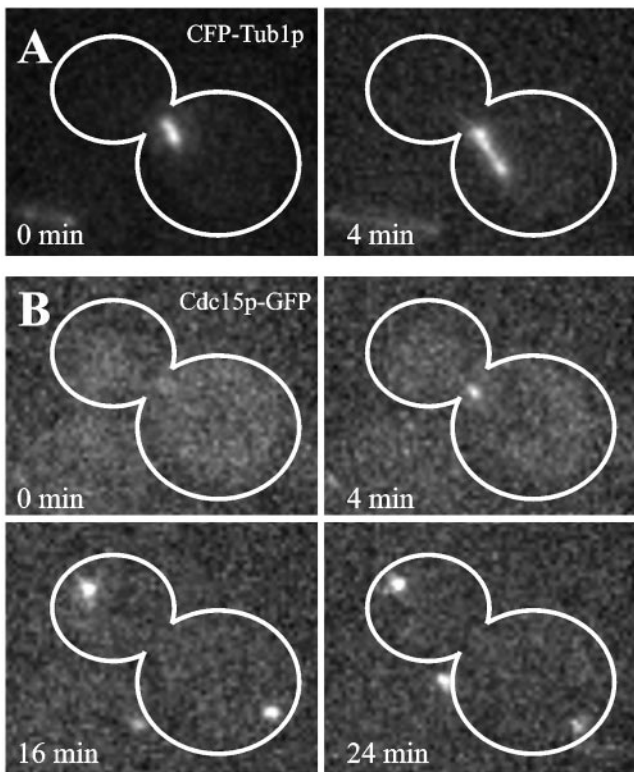
Figure 5. Live cell localization of Cdc15p-GFP during anaphase (Bar, 5 μm). (A) Mitotic spindle elongation marked by CFP-Tub1p. The frame before spindle extension, visualized by CFP-Tub1p, was designated as the initial time point in this experiment. Penetration of the bud neck occurred at $t = 4$ min. (B) Cdc15p-GFP localization during anaphase spindle elongation. (0 min) Cdc15p-GFP does not localize to SPBs. (4 min) On mitotic spindle elongation Cdc15p-GFP accumulates on the dSPB. (16 min, 24 min) Accumulation of Cdc15p-GFP occurred on both SPBs in late anaphase.

anaphase onset (Figure 6A). Measuring the fluorescence intensity of Bub2p-GFP in individual cells during spindle elongation demonstrated Bub2p-GFP levels decreased from the dSPB in either midanaphase (Figure 6B) or when the spindle pole reached the distal daughter cell cortex in late anaphase (Figure 6C). The quantitative fluorescence intensity measurements of Tem1p-GFP, Spc29p-GFP, and Bub2p-GFP are plotted schematically in Figure 6D for direct comparison of these probes. From these quantitative data, we conclude Bub2p is lost from the dSPB in mid-to-late anaphase when Tem1p localization becomes most abundant.

Compartmentalization of Lte1p Is Restricted to the Daughter Cell Cortex

The inhibitory activity of the spindle position checkpoint on Tem1p may be counteracted by Lte1p once the dSPB segregates into the bud (Bardin *et al.*, 2000; Pereira *et al.*, 2000). The increase in Tem1p at the dSPB in the bud could result from an interaction between Tem1p and a large fraction of Lte1p in the bud cytosol that activates mitotic exit. Alternatively, the majority of Lte1p could localize to the bud cortex predicting Tem1p-Lte1p interactions rely on dynamic protein exchange in the cytoplasm. To determine the localization of the MEN activator Lte1p in more detail, we introduced three tandem copies of GFP at the C-terminus of Lte1p (Lte1p-3xGFP). Lte1p-3xGFP was characterized in

wild-type cells by deconvolution microscopy and three-dimensional reconstruction (Figure 7, Supplementary Movie 3). Three-dimensional lateral projections of 23 cells showed that all of the detectable Lte1p-3xGFP is unevenly distributed to the periphery of the cell adjacent to the plasma membrane (our unpublished results). Because the majority of Lte1p localizes to the bud cortex, Tem1p-Lte1p interactions must be dynamic if Lte1p affects Tem1p localization at the dSPB.

Characterization of Tem1p-GFP Dynamics by FRAP

We examined Tem1p at the dSPB in more detail to understand the mechanisms that underlie Tem1p dynamics and accumulation during activation of mitotic exit. The increase in Tem1p-GFP at the dSPB in late anaphase as well as the localization of Lte1p to the bud cortex suggests Tem1p is dynamic and exchanges between the cytoplasm and spindle pole. Alternatively, Tem1p could bind tightly to the dSPB in late anaphase. To determine if Tem1p is dynamic, we photobleached Tem1p-GFP in late anaphase during mitotic exit and quantified Tem1p-GFP recovery to the dSPB (Figure 8, A and B). Kinetic analysis of recovery indicated a fast and a slow phase to Tem1p-GFP recovery. An example of a single exponential and a biphasic fit to the experimental data is shown in Figure 8, C and D. The fast fraction of Tem1p-GFP has an average half-recovery time ($t_{1/2}$) of 4.50 ± 2.29 s (mean $\pm$ SD) with 56.5% of the recovery to the dSPB due to the fast fraction (Table 3). The slow fraction of Tem1p-GFP had a $t_{1/2}$ of 133 ± 85.5 s and 43.5% recovery to the dSPB was contributed by the slow fraction (Table 3). The total recovery (R) of Tem1p-GFP to the dSPB was 61.2% over the 5-min imaging interval.

The high temporal resolution required to resolve the two kinetic phases of Tem1p-GFP limited image acquisition to single Z-planes. To determine if shifts in the Z-focal plane of the mitotic spindle or subtle photobleaching during image acquisition resulted in only ~61% fluorescence recovery to the dSPB, we photobleached cells and acquired a single five-plane Z-series at 5 and 10 min after the laser pulse. The calculated R value of Tem1p-GFP at the dSPB using this approach was 96% ($n = 5$), indicating that Tem1p at the dSPB exchanges nearly completely with the cytoplasmic pool within 10 min. Thus, Tem1p is dynamic at the dSPB in late anaphase.

Tem1p-GFP Distribution Responds to Active Spindle Positioning

The dynamics of Tem1p at the dSPB may reflect the ability of Tem1p to respond to positional cues during spindle orientation. In wild-type cells Tem1p preferentially localizes to the dSPB as it positions along the mother-bud axis (Figure 3A). Tem1p persistence at the dSPB in anaphase, instead of just an increase in localization, may be the key to signaling mitotic exit. Oscillations of wild-type preanaphase spindles within the mother cell before spindle alignment and establishment of Tem1p-GFP asymmetry are rare. To examine Tem1p-GFP on spindle poles orienting along the mother-bud axis, we examined Tem1p-GFP in *kar9Δ* mutants defective in nuclear positioning (Miller and Rose, 1998). Tem1p-GFP transiently accumulated on either spindle pole in these mutants when the spindle was approximately parallel to the bud neck (Figure 9A, Supplementary Movie 4). Preferential Tem1p-GFP distributions on a single SPB before anaphase were not sufficient for mitotic exit because the cell remained arrested until the spindle reoriented along the mother-bud axis (Figure 9A). Further, passage of the spindle through the bud neck did not irreversibly increase Tem1p-GFP. The spindle could transiently enter the bud causing an increase
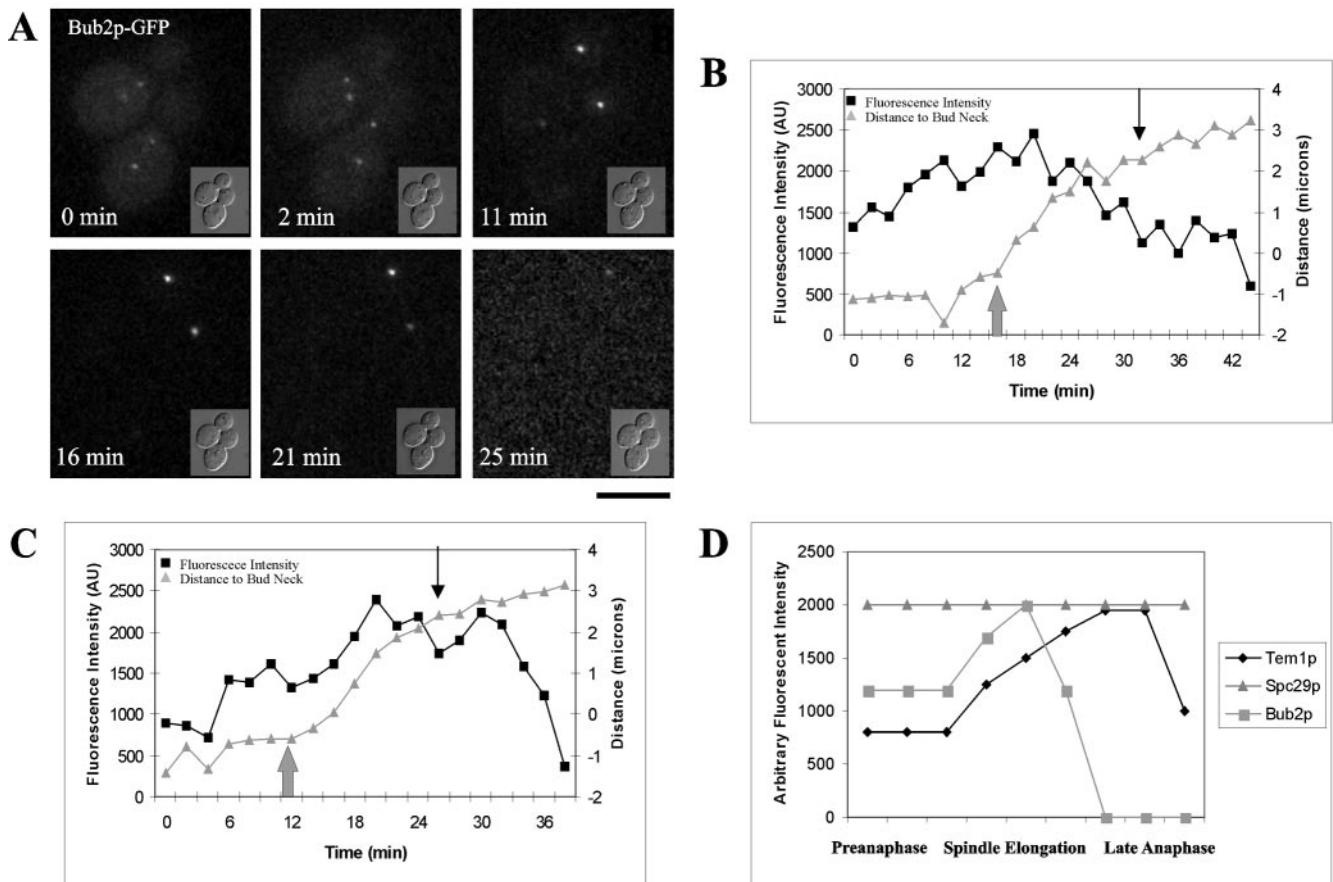
Figure 6. Bub2p-GFP fluorescence intensity analysis. (A) Bub2p-GFP localization in living cells. DIC image is inset to fluorescence image (Bar, 5 μm for fluorescence image). (0 min, 2 min) Bub2p-GFP localizes to both SPBs. (11 min, 16 min) Bub2p-GFP increases on the dSPB and is lost from the mSPB. (21 min, 25 min) Bub2p-GFP is lost from the dSPB. (B) Example of Bub2p-GFP fluorescence intensity decrease on the dSPB in midanaphase. Large gray arrow, spindle elongation; black arrow, maximum spindle extension. Black squares, fluorescence intensity in arbitrary units (AU); gray triangles, distance to bud neck in micrometers. (C) Example of Bub2p-GFP fluorescence intensity decrease on the dSPB in late anaphase. Large gray arrow, spindle elongation; black arrow, maximum spindle extension. Black squares, fluorescence intensity in arbitrary units (AU); gray triangles, distance to bud neck in microns. (D) Summary of Tem1p-GFP, Spc29p-GFP, and Bub2p-GFP quantitative measurements. Arbitrary fluorescence intensity scale is derived from the approximate fluorescence intensity of each probe as measured in the previous figures.

of Tem1p-GFP on the dSPB and then move back into the mother cell resulting in decreased fluorescence intensity (Figure 9A, 34 and 38 min). On spindle elongation, Tem1p-GFP accumulated on the SPB positioned in the daughter cell (Figure 9A, 62 min).

By designating the SPB that eventually enters the bud as the dSPB and the SPB that is retained in the mother cell as the mSPB, we plotted the change in Tem1p-GFP fluorescence intensity for each SPB as well as the distance from the SPB to the bud neck (Figure 9B, dSPB, and C, mSPB). The fluorescence intensity of the dSPB dramatically increased when penetration into the daughter cell occurred. Additionally, the dSPB appeared to stabilize in fluorescence intensity near the bud neck before penetration into the daughter cell, similar to the situation during wild-type spindle positioning in preanaphase. Finally, the persistence of Tem1p on the dSPB is a consequence of entry into the bud and presumably signals mitotic exit.

Lte1p Is Required for Tem1p-GFP Localization during Mitotic Exit

How Lte1p at the bud cortex may regulate dynamic Tem1p in the cytoplasm is still unclear. The restriction of Lte1p to

the bud during preanaphase and early anaphase could contribute to the specific accumulation of Tem1p on the dSPB upon penetration into the bud. To determine if Lte1p contributes to Tem1p-GFP localization during mitotic exit, we compared the fluorescence intensity of Tem1p-GFP on the dSPB in late anaphase between wild-type strains and $lte1\Delta$ cells (Figure 10A). As a control, we deleted *ASE1*. Deletion of *ASE1* results in a delay in anaphase onset (Schuyler *et al.*, 2003) but does not change the timing of anaphase or mitotic exit (Figures 1 and 2), predicting Tem1p-GFP fluorescence intensity should not be different from wild-type levels. The fluorescence intensity of Tem1p-GFP in $ase1\Delta$ cells was not significantly different from wild-type cells, with the ratio of Tem1p-GFP fluorescence intensity in the mutant cells to Tem1p-GFP fluorescence intensity in wild-type cells equaling 1.08:1.00 (p > 0.10). In contrast, Tem1p-GFP is significantly reduced in $lte1\Delta$ cells grown at 32°C (fluorescence intensity ratio 0.54:1.00; $p < 1 \times 10^{-7}$). Analysis of Bub2p-GFP on the dSPB in wild-type and $lte1\Delta$ cells grown at 32°C indicated there was no significant loss of Bub2p-GFP fluorescence intensity (our unpublished results). Thus, Tem1p localization to the dSPB is specifically promoted by Lte1p in vivo.
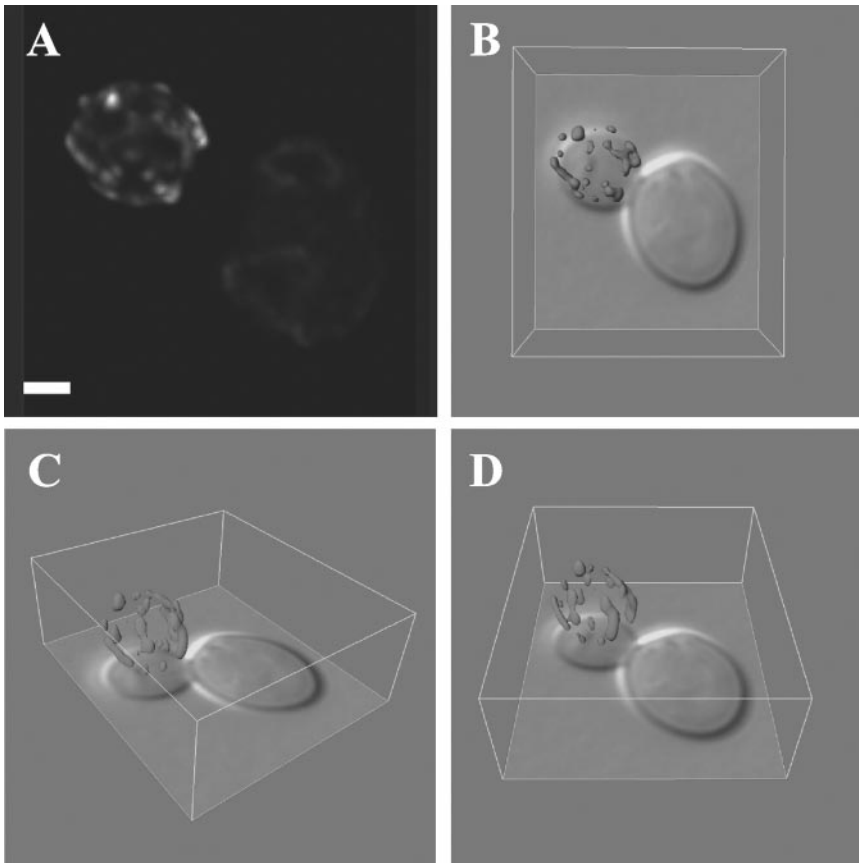
Figure 7. Native level Lte1p-3xGFP is localized to the daughter cell cortex. (A) An example of a deconvolved cell in two dimensions (Bar, 2 μm). (B–D) Projections of the three-dimensional image show that all of the Lte1p-3xGFP is localized to the periphery of the cell next to the cortex and is not associated with any internal structure within the bud.

Microtubule Motor Proteins and Kar9p Regulate Tem1p-GFP Localization in Late Anaphase

Because Tem1p-GFP fluorescence intensity varies with spindle positioning (Figure 9), it is possible that factors involved in nuclear orientation can also moderate the amount of Tem1p-GFP found on spindle poles. By analyzing Tem1p-GFP on the dSPB in late anaphase of properly positioned spindles, we could determine the effect of spindle orientation factors on Tem1p-GFP abundance (Figure 10B). Deletion of the cytoplasmic dynein heavy chain (*DHC1*) significantly decreased Tem1p-GFP fluorescence intensity on the dSPB of properly elongated spindles in the bud (fluorescence intensity ratio = 0.63:1.00; p < 1 × 10^{-4}). In *dhc1Δ* cells Bub2p-GFP fluorescence intensity was not altered significantly in any stage of the cell cycle (our unpublished results), indicating the loss of fluorescence is specific for Tem1p. Tem1p-GFP fluorescence intensity was reduced by deleting the microtubule motor protein *KIP2* (fluorescence intensity ratio = 0.72:1.00; p < 0.013) and spindle orientation factor *KAR9* (fluorescence intensity ratio = 0.76:1.00; p < 0.02). In contrast, loss of Bud6p, a cortical protein involved in Kar9p-independent spindle orientation (Segal *et al.*, 2002) had no effect on the accumulation of Tem1p-GFP at the dSPB in late anaphase (fluorescence intensity ratio = 1.00:1.00; p > 0.10). Finally, deletion of the microtubule motor protein *KIP3* resulted in increased Tem1p-GFP localization to the dSPB compared with wild-type controls in late anaphase (fluorescence intensity ratio = 1.43:1.00, p < 0.01). Thus, Dhc1p and other spindle orientation factors regulate Tem1p abundance and persistence in late anaphase.

DISCUSSION

Using quantitative live cell microscopy we have investigated the dynamics of MEN proteins during mitotic exit. Passage of the spindle pole into the bud, and not contact with the distal bud cortex, signaled mitotic exit (Figures 1 and 2). Positioning of the dSPB at the bud neck and subsequent entry into the daughter cell resulted in the increased accumulation of Tem1p at the dSPB relative to the mSPB (Figures 3 and 4). These data indicate that Tem1p on the dSPB does not need to contact the distal bud cortex to either facilitate Tem1p accumulation on the dSPB or to activate mitotic exit. The increased Tem1p localization to the dSPB once in the bud could merely reflect a programmed increase in Tem1p protein levels that peak in telophase (Bardin *et al.*, 2000) or SPB maturation during mitosis. Using mal-oriented spindles, we showed that positioning along the mother-bud axis rather than the time spent in preanaphase or anaphase generates Tem1p-GFP asymmetry (Figures 3C and 9). Additionally, increases in fluorescence intensity occurred when the spindle pole entered the daughter cell (Figures 3C and 9). Thus, Tem1p localization responds to the spatial movement of the mitotic spindle and entry into the bud.

Determining the mechanism of Tem1p accumulation on the dSPB requires information about both the factors that regulate Tem1p localization and the dynamics of Tem1p. To understand the regulation of Tem1p-GFP abundance on the dSPB, we examined Tem1p-GFP in *lte1Δ* cells. The majority of Lte1p localizes to the bud cortex and could promote Tem1p localization to the dSPB in the bud (Figure 7). In the absence of Lte1p the abundance of Tem1p is significantly diminished (Figure 10A). Importantly, this indicates that if a
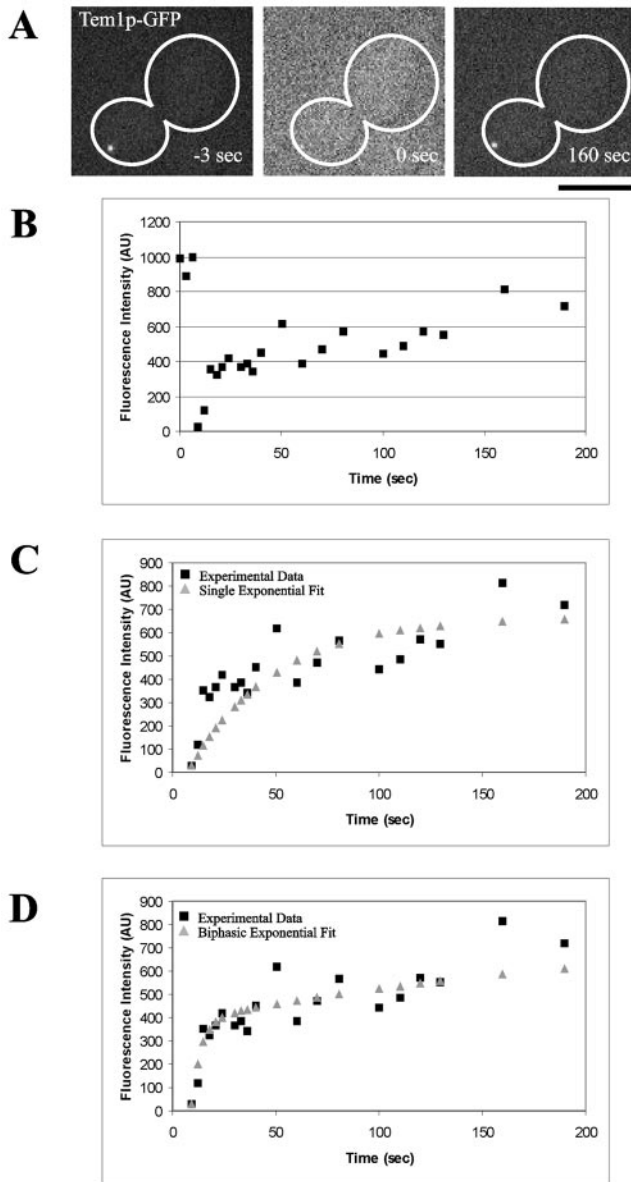
Figure 8. FRAP of Tem1p-GFP in late anaphase. Fluorescence intensity is recorded in arbitrary units (AU). (A) Prebleach $t = -3$ s; time of photobleaching $t = 0$ s; recovery $t = 160$ s (Bar, 5 μm). (B) Quantified recovery of fluorescence for the same dSPB photobleached in A. (C) Comparison of experimental data (black squares) with single exponential best-fit data (gray triangles). (D) Comparison of experimental data (black squares) with biphasic exponential best fit data (gray triangles). See MATERIALS AND METHODS for details of analysis.

Table 3. FRAP of Tem1p-GFP on the anaphase dSPB

Probe	k_f	$t_{1/2}f$	$f_f{}^a$	k_s	$t_{1/2}s$	f_s	R^b
Tem1p-GFP	0.203	4.50	56.5	0.0103	133	43.5	62.1

[a] All fraction of recovery values are given as percentages ($f \times 100$) of the total recovery R.

[b] R was corrected for the amount of Tem1p-GFP photobleached by the laser pulse (see MATERIALS AND METHODS).

been shown to exist during mitotic exit (Castillon *et al.*, 2003). Lte1p has been linked with Ras function and the Lte1p GEF domain is not necessary for mitotic exit (Yoshida *et al.*, 2003). Our data indicate that Lte1p may function to promote Tem1p localization at the dSPB. One possibility is that Tem1p localization is controlled by Lte1p independently of Lte1p GEF activity. Tem1p has a high rate of GDP release in vitro (Geymonat *et al.*, 2002), suggesting the intrinsic nucleotide dynamics of Tem1p may not need to be supplemented by Lte1p GEF activity to drive mitotic exit. Lte1p could serve as a redundant mechanism at physiological temperatures to ensure Tem1p localizes to the dSPB in sufficient amounts to interact with Cdc15p for mitotic exit to occur.

To examine Tem1p dynamics and test if Tem1p is stable or exchanges with the cytoplasmic protein pool at the dSPB in late anaphase, we photobleached Tem1p-GFP. This analysis revealed two kinetic fractions of Tem1p at the dSPB in late anaphase (Figure 8, Table 3). What are possible explanations for the biphasic recovery of Tem1p-GFP to the dSPB? Local diffusion of Tem1p to the dSPB may account for the fast phase, and a second mechanism may account for the slow phase, perhaps interactions with different binding partners including Bub2p, Cdc15, or other proteins. The two fractions could reflect the nucleotide hydrolysis states of Tem1p during mitotic exit. Alternatively, the two phases may represent interactions with different subsets of proteins at the dSPB, such as Tem1p-Cdc15p and Tem1p-Bub2p interactions, or transport of Tem1p by different microtubule motor proteins. Although the nature of the biphasic recovery remains unknown, our FRAP measurements demonstrate Tem1p at the dSPB rapidly exchanges with the cytoplasmic protein pool.

Tem1p protein exchange at the dSPB as well as the positional changes in Tem1p-GFP fluorescence intensity during spindle positioning (Figures 3 and 9) suggest that pulling or pushing forces could result in rapid changes in Tem1p abundance. In wild-type cells, microtubules from the mSPB probe the mother cell cortex rather than forming prolonged attachments that promote force generation (Figure 4; Shaw *et al.*, 1997b). The transient localization of Tem1p-GFP at the mSPB may reflect the lack of microtubule attachments that generate force in the mother cell. A prediction from our data is that there is greater net force on the dSPB during mitosis, especially in anaphase. Similarly, dynein generates a dominant force to move the nucleus through the bud neck (Yeh *et al.*, 1995, 2000) and Dhc1p is needed to concentrate Tem1p-GFP on the dSPB in late anaphase (Figure 10B). This suggests Tem1p localization depends on either microtubule dynamics, transport by microtubule motor proteins, or force generation. Because the plus-end motor Kip2p also decreases Tem1p-GFP at the dSPB, a more general defect in either nuclear migration or microtubule dynamics likely regulate Tem1p abundance at the dSPB. Deletion of *KIP3* results in an increase in Tem1p-GFP on the dSPB. This result could be an indirect effect due to a delay in the cell cycle in
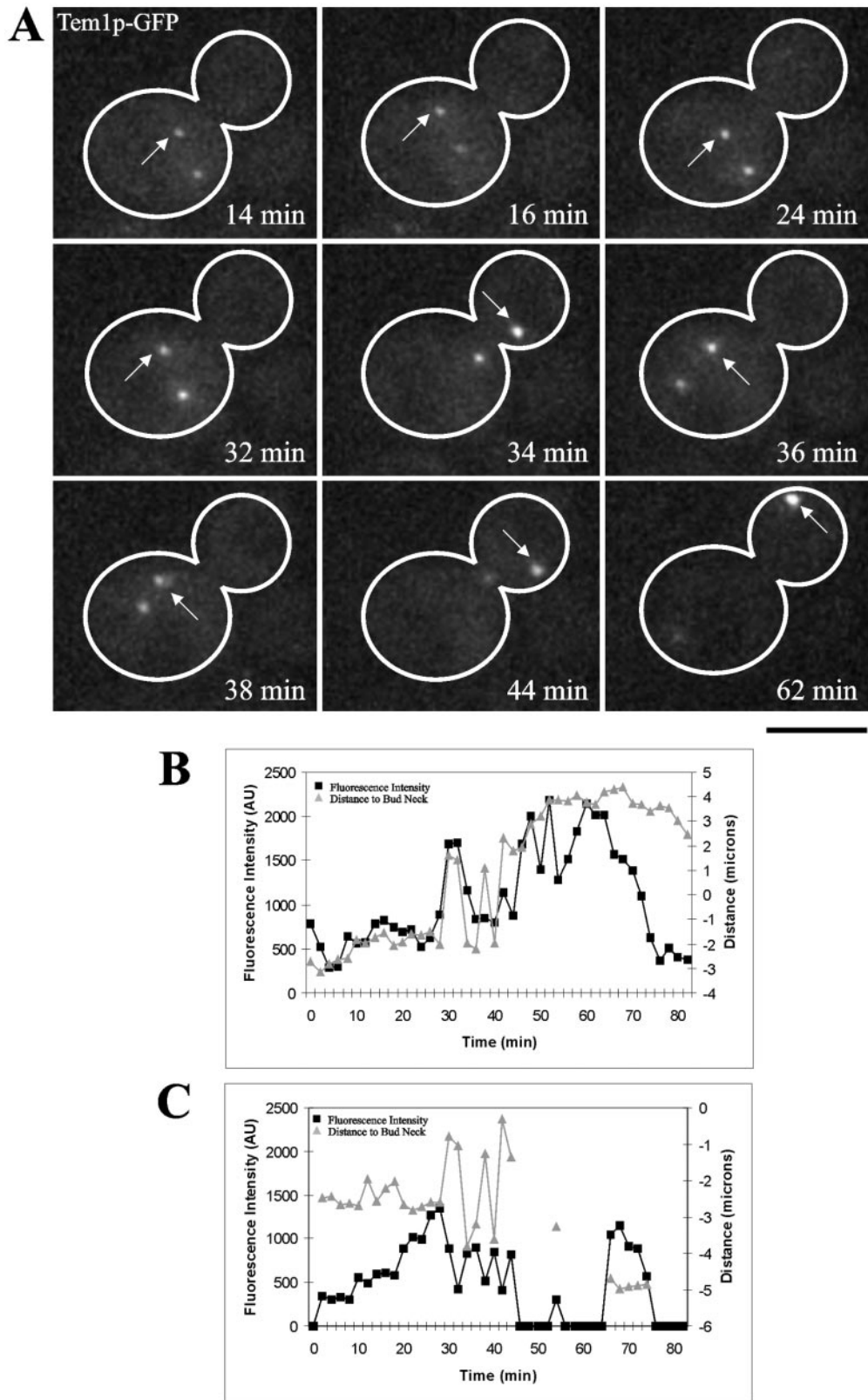
"threshold" level of Tem1p on the dSPB exists that must be surpassed before mitotic exit is activated, this threshold is low in *lte1Δ* mutants. Because dSPB penetration into the bud results in activation of mitotic exit, Tem1p-Lte1p interactions either have to occur in the cytoplasm or Tem1p interacts with Lte1p at the bud cortex and then relocalizes to the dSPB. Because there is no evidence that Tem1p localizes to the bud cortex, most likely Tem1p and Lte1p interact in the cytoplasm, suggesting Lte1p may be dynamic and exchange between the bud cortex and the cytoplasmic protein pool. In support of this hypothesis, a cytoplasmic pool of Lte1p has

Figure 9. Spindle reorientation results in accumulation of Tem1p-GFP on the SPB that enters the bud in *kar9Δ* mutants. (A) Selected frames from a movie showing changes in Tem1p-GFP fluorescence intensity during active reorientation of mitotic spindle. Arrow denotes SPB that will enter bud (Bar, 5 µm). (B) Quantified changes of Tem1p-GFP fluorescence in arbitrary units (AU; black squares) and distance from the bud neck in microns (gray triangles) for the dSPB in A. (C) Measured changes of Tem1p-GFP fluorescence in arbitrary units (AU; black squares) and distance from the bud neck in microns (gray triangles) for the mSPB from the cell in A. The line gap in distance data points correlates with images where no mSPB signal was detected; in these cases the fluorescence intensity was recorded as zero.
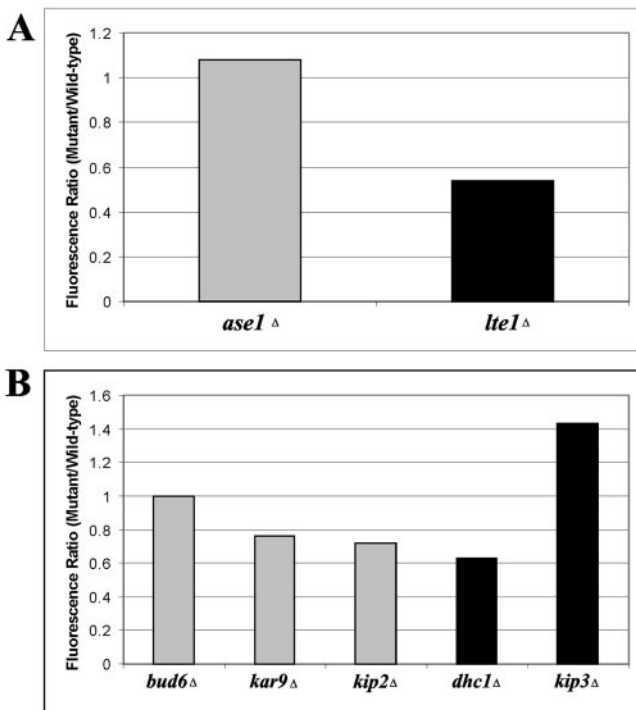
Figure 10. Fluorescence ratio of Tem1p-GFP accumulation on the dSPB in late anaphase cells. (A) The fluorescence intensity on the dSPB of Tem1p-GFP in *ase1*Δ or *lte1*Δ mutants was divided by the fluorescence intensity of wild-type Tem1p-GFP in late anaphase to generate a fluorescence intensity ratio. Gray bar indicates nonsignificant differences from wild-type; black bar indicates significant difference from wild-type. At least 25 individual cells were measured and averaged for each strain. (B) Tem1p-GFP fluorescence intensity ratio in spindle orientation factors and microtubule motor mutant cells. Gray bars indicate nonsignificant deviation from wild-type fluorescence intensity and black bars denote significant changes from wild-type fluorescence intensity. At least 25 individual cells were measured and averaged for each strain.

*kip3*Δ mutants (Straight *et al.*, 1998), a phenotype we have seen in other mutants delayed in the cell cycle (our unpublished results). How do Dhc1p and Kip2p promote Tem1p abundance at the dSPB? One possibility is that both Dhc1p and Kip2p transport Tem1p in different directions along the microtubules. Alternatively, forces or tension at the dSPB may be a general mechanism that regulates Tem1p accumulation. However, the molecular mechanism of Tem1p loss from the dSPB in *dhc1*Δ cells requires further study.

After the increased accumulation of Tem1p at dSPB upon penetration of the bud neck, Cdc15p initially accumulated on the dSPB and subsequently localized to both SPBs (Figure 5), whereas Bub2p decreased from spindle poles in mid-to-late anaphase (Figure 6). Coupling this data with our observations on Tem1p, we can envision a model for mitotic exit that integrates protein dynamics. In wild-type cells with properly positioned preanaphase spindles, Tem1p accumulation is antagonized by Bub2p at the dSPB. Bub2p inhibition prevents Tem1p and Cdc15p accumulation at the dSPB. Factors that promote Tem1p accumulation may include Dhc1p, Lte1p, tension or force, unknown accessory factors, and position relative to the bud. The positional dependence for Tem1p localization to the dSPB may also be due to a gradient of Tem1p in the GTP bound form that is found in the bud. On anaphase onset and dSPB penetration into the

bud a switch is activated allowing Cdc15p to accumulate on the dSPB. Because Cdc15p is activated, Bub2p localization to the dSPB is not favored. A feedback loop could exist at this point, where Cdc15p promotes Tem1p accumulation to allow more Cdc15p accumulation at the dSPB, while Cdc15p prevents Bub2p binding to the dSPB. Tem1p and Cdc15p accumulate on the dSPB to signal mitotic exit, whereas Bub2p is either released from the dSPB or has its binding sites at the dSPB filled by the Tem1p-Cdc15p complex. The switch to persistent Tem1p-Cdc15p signaling allows mitotic exit to proceed.

In conclusion, we provide evidence that the accumulation of dynamic Tem1p as spindle poles pass the bud neck and a change in Bub2p distribution correlates with mitotic exit. The dynamic nature of Tem1p allows it to respond quickly to changes within the cell, making Tem1p an ideal spatial sensor in vivo. The discovery of a protein intimately linked to both spindle positioning and activating mitotic exit will allow dissection of the connections between forces that position structures and cell signaling networks during the cell cycle.

REFERENCES

Adames, N.R., Oberle, J.R., and Cooper, J.A. (2001). The surveillance mechanism of the spindle position checkpoint in yeast. J. Cell Biol. *153*, 159–168.

Alexandru, G., Zachariae, W., Schleiffer, A., and Nasmyth, K. (1999). Sister chromatid separation and chromosome re-duplication are regulated by different mechanisms in response to spindle damage. EMBO J. *18*, 2707–2721.

Bardin, A.J., and Amon, A. (2001). Men and sin: what's the difference? Nat. Rev. Mol. Cell. Biol. *2*, 815–826.

Bardin, A.J., Visintin, R., and Amon, A. (2000). A mechanism for coupling exit from mitosis to partitioning of the nucleus. Cell *102*, 21–31.

Bi, E., Maddox, P., Lew, D.J., Salmon, E.D., McMillan, J.N., Yeh, E., and Pringle, J.R. (1998). Involvement of an actomyosin contractile ring in Saccharomyces cerevisiae cytokinesis. J. Cell Biol. *142*, 1301–1312.

Bi, E., and Pringle, J.R. (1996). ZDS1 and ZDS2, genes whose products may regulate Cdc42 in Saccharomyces cerevisiae. Mol. Cell. Biol. *16*, 5264–5275.

Bloecher, A., Venturi, G.M., and Tatchell, K. (2000). Anaphase spindle position is monitored by the BUB2 checkpoint. Nat. Cell Biol. *2*, 556–558.

Byers, B., and Goetsch, L. (1975). Behavior of spindles and spindle plaques in the cell cycle and conjugation of Saccharomyces cerevisiae. J. Bacteriol. *124*, 511–523.

Castillon, G.A., Adames, N.R., Rosello, C.H., Seidel, H.S., Longtine, M.S., Cooper, J.A., and Heil-Chapdelaine, R.A. (2003). Septins have a dual role in controlling mitotic exit in budding yeast. Curr. Biol. *13*, 654–658.

Daum, J.R., Gomez-Ospina, N., Winey, M., and Burke, D.J. (2000). The spindle checkpoint of Saccharomyces cerevisiae responds to separable microtubule-dependent events. Curr. Biol. *10*, 1375–1378.

Fesquet, D., Fitzpatrick, P.J., Johnson, A.L., Kramer, K.M., Toyn, J.H., and Johnston, L.H. (1999). A Bub2p-dependent spindle checkpoint pathway regulates the Dbf2p kinase in budding yeast. EMBO J. *18*, 2424–2434.

Fraschini, R., Formenti, E., Lucchini, G., and Piatti, S. (1999). Budding yeast Bub2 is localized at spindle pole bodies and activates the mitotic checkpoint via a different pathway from Mad2. J. Cell Biol. *145*, 979–991.

Geymonat, M., Spanos, A., Smith, S.J., Wheatley, E., Rittinger, K., Johnston, L.H., and Sedgwick, S.G. (2002). Control of mitotic exit in budding yeast. In

vitro regulation of Tem1 GTPase by Bub2 and Bfa1. J. Biol. Chem. *277,* 28439–28445.

Goldstein, A.L., and McCusker, J.H. (1999). Three new dominant drug resistance cassettes for gene disruption in Saccharomyces cerevisiae. Yeast *15,* 1541–1553.

Howell, B.J., Hoffman, D.B., Fang, G., Murray, A.W., and Salmon, E.D. (2000). Visualization of Mad2 dynamics at kinetochores, along spindle fibers, and at spindle poles in living cells. J. Cell Biol. *150,* 1233–1250.

Hoyt, M.A. (2000). Exit from mitosis: spindle pole power. Cell *102,* 267–270.

Hoyt, M.A., Totis, L., and Roberts, B.T. (1991). S. cerevisiae genes required for cell cycle arrest in response to loss of microtubule function. Cell *66,* 507–517.

Kilmartin, J.V., and Adams, A.E. (1984). Structural rearrangements of tubulin and actin during the cell cycle of the yeast Saccharomyces. J. Cell Biol. *98,* 922–933.

Kosco, K.A., Pearson, C.G., Maddox, P.S., Wang, P.J., Adams, I.R., Salmon, E.D., Bloom, K., and Huffaker, T.C. (2001). Control of microtubule dynamics by Stu2p is essential for spindle orientation and metaphase chromosome alignment in yeast. Mol. Biol. Cell *12,* 2870–2880.

Lee, L., Klee, S.K., Evangelista, M., Boone, C., and Pellman, D. (1999). Control of mitotic spindle position by the Saccharomyces cerevisiae formin Bni1p. J. Cell Biol. *144,* 947–961.

Li, R. (1999). Bifurcation of the mitotic checkpoint pathway in budding yeast. Proc. Natl. Acad. Sci. USA *96,* 4989–4994.

Li, Y.Y., Yeh, E., Hays, T., and Bloom, K. (1993). Disruption of mitotic spindle orientation in a yeast dynein mutant. Proc. Natl. Acad. Sci. USA *90,* 10096–10100.

Longtine, M.S., McKenzie, A., 3rd, Demarini, D.J., Shah, N.G., Wach, A., Brachat, A., Philippsen, P., and Pringle, J.R. (1998). Additional modules for versatile and economical PCR-based gene deletion and modification in Saccharomyces cerevisiae. Yeast *14,* 953–961.

Maddox, P.S., Bloom, K.S., and Salmon, E.D. (2000). The polarity and dynamics of microtubule assembly in the budding yeast Saccharomyces cerevisiae. Nat. Cell Biol. *2,* 36–41.

McCollum, D., and Gould, K.L. (2001). Timing is everything: regulation of mitotic exit and cytokinesis by the MEN and SIN. [erratum appears in Trends Cell Biol. 2001 *11*(4), 166.]. Trends Cell Biol. *11,* 89–95.

Miller, R.K., Heller, K.K., Frisen, L., Wallack, D.L., Loayza, D., Gammie, A.E., and Rose, M.D. (1998). The kinesin-related proteins, Kip2p and Kip3p, function differently in nuclear migration in yeast. Mol. Biol. Cell *9,* 2051–2068.

Miller, R.K., and Rose, M.D. (1998). Kar9p is a novel cortical protein required for cytoplasmic microtubule orientation in yeast. J. Cell Biol. *140,* 377–390.

Pellman, D., Bagget, M., Tu, Y.H., Fink, G.R., and Tu, H. (1995). Two microtubule-associated proteins required for anaphase spindle movement in Saccharomyces cerevisiae. [erratum appears in J. Cell Biol. 1995 *131*(2), 561.]. J. Cell Biol. *130,* 1373–1385.

Pereira, G., Hofken, T., Grindlay, J., Manson, C., and Schiebel, E. (2000). The Bub2p spindle checkpoint links nuclear migration with mitotic exit. Mol. Cell *6,* 1–10.

Pereira, G., Tanaka, T.U., Nasmyth, K., and Schiebel, E. (2001). Modes of spindle pole body inheritance and segregation of the Bfa1p-Bub2p checkpoint protein complex. EMBO J. *20,* 6359–6370.

Ro, H.S., Song, S., and Lee, K.S. (2002). Bfa1 can regulate Tem1 function independently of Bub2 in the mitotic exit network of Saccharomyces cerevisiae. Proc. Natl. Acad. Sci. USA *99,* 5436–5441.

Robinow, C.F., and Marak, J. (1966). A fiber apparatus in the nucleus of the yeast cell. J. Cell Biol. *29,* 129–151.

Rose, A.B., and Broach, J.R. (1990). Propagation and expression of cloned genes in yeast: 2-microns circle-based vectors. Methods Enzymol. *185,* 234–279.

Salmon, E.D., Leslie, R.J., Saxton, W.M., Karow, M.L., and McIntosh, J.R. (1984). Spindle microtubule dynamics in sea urchin embryos: analysis using a fluorescein-labeled tubulin and measurements of fluorescence redistribution after laser photobleaching. J. Cell Biol. *99,* 2165–2174.

Saxton, W.M., Stemple, D.L., Leslie, R.J., Salmon, E.D., Zavortink, M., and McIntosh, J.R. (1984). Tubulin dynamics in cultured mammalian cells. J. Cell Biol. *99,* 2175–2186.

Schuyler, S.C., Liu, J.Y., and Pellman, D. (2003). The molecular function of Ase1p: evidence for a MAP-dependent midzone-specific spindle matrix. J. Cell Biol. *160,* 517–528.

Segal, M., Bloom, K., and Reed, S.I. (2002). Kar9p-independent microtubule capture at Bud6p cortical sites primes spindle polarity before bud emergence in *Saccharomyces cerevisiae.* Mol. Biol. Cell *13,* 4141–4155.

Shaw, S.L., Yeh, E., Bloom, K., and Salmon, E.D. (1997a). Imaging green fluorescent protein fusion proteins in Saccharomyces cerevisiae. Curr. Biol. *7,* 701–704.

Shaw, S.L., Yeh, E., Maddox, P., Salmon, E.D., and Bloom, K. (1997b). Astral microtubule dynamics in yeast: a microtubule-based searching mechanism for spindle orientation and nuclear migration into the bud. J. Cell Biol. *139,* 985–994.

Shirayama, M., Matsui, Y., Tanaka, K., and Toh-e, A. (1994). Isolation of a CDC25 family gene, MSI2/LTE1, as a multicopy suppressor of ira1. Yeast *10,* 451–461.

Sikorski, R.S., and Hieter, P. (1989). A system of shuttle vectors and yeast host strains designed for efficient manipulation of DNA in Saccharomyces cerevisiae. Genetics *122,* 19–27.

Straight, A.F., Marshall, W.F., Sedat, J.W., and Murray, A.W. (1997). Mitosis in living budding yeast: anaphase A but no metaphase plate. Science *277,* 574–578.

Straight, A.F., Sedat, J.W., and Murray, A.W. (1998). Time-lapse microscopy reveals unique roles for kinesins during anaphase in budding yeast. J. Cell Biol. *143,* 687–694.

Tirnauer, J.S., O'Toole, E., Berrueta, L., Bierer, B.E., and Pellman, D. (1999). Yeast Bim1p promotes the G1-specific dynamics of microtubules. J. Cell Biol. *145,* 993–1007.

Visintin, R., and Amon, A. (2001). Regulation of the mitotic exit protein kinases Cdc15 and Dbf2. Mol. Biol. Cell *12,* 2961–2974.

Wach, A., Brachat, A., Pohlmann, R., and Philippsen, P. (1994). New heterologous modules for classical or PCR-based gene disruptions in Saccharomyces cerevisiae. Yeast *10,* 1793–1808.

Wadsworth, P., and Salmon, E.D. (1986). Microtubule dynamics in mitotic spindles of living cells. Ann. NY Acad. Sci. *466,* 580–592.

Yeh, E., Skibbens, R.V., Cheng, J.W., Salmon, E.D., and Bloom, K. (1995). Spindle dynamics and cell cycle regulation of dynein in the budding yeast, Saccharomyces cerevisiae. J. Cell Biol. *130,* 687–700.

Yeh, E., Yang, C., Chin, E., Maddox, P., Salmon, E.D., Lew, D.J., and Bloom, K. (2000). Dynamic positioning of mitotic spindles in yeast: role of microtubule motors and cortical determinants. Mol. Biol. Cell *11,* 3949–3961.

Yoshida, S., Ichihashi, R., and Toh-e, A. (2003). Ras recruits mitotic exit regulator Lte1 to the bud cortex in budding yeast. J. Cell Biol. *161,* 889–897.